THE JOURNAL OF BIOLOGICAL CHEMISTRY VOL. 285, NO. 6, pp. 3840–3849, February 5, 2010

Fbxo45, a Novel Ubiquitin Ligase, Regulates Synaptic Activity*[S]

Received for publication, July 18, 2009, and in revised form, December 1, 2009 Published, JBC Papers in Press, December 7, 2009, DOI 10.1074/jbc.M109.046284

Hirobumi Tada[‡§¶], Hirotaka James Okano[‡‖1], Hiroshi Takagi[**], Shinsuke Shibata[‡], Ikuko Yao[**], Masaki Matsumoto[‡‡§§], Toru Saiga[‡‡§§], Keiichi I. Nakayama[‡‡§§], Haruo Kashima[¶¶], Takuya Takahashi[§], Mitsutoshi Setou[‖‖2], and Hideyuki Okano[‡¶‖3]**

From the [‡]Department of Physiology, the [¶]Bridgestone Laboratory of Developmental and Regenerative Neurobiology, and the [¶¶]Department of Neuropsychiatry, Keio University School of Medicine, Tokyo 160-8582, the [§]Department of Physiology, Yokohama City University School of Medicine, Kanagawa 236-0004, [‖]SORST (Solution Oriented Research for Science and Technology) and [§§]CREST (Core Research for Evolutional Science and Technology), the Japan Science and Technology Agency, Saitama 332-0012, the [**]Laboratory for Molecular Gerontology, Mitsubishi Kagaku Institute of Life Sciences Setou Group, Tokyo 194-8511, the [‡‡]Department of Molecular and Cellular Biology, Medical Institute of Bioregulation, Kyushu University, Fukuoka 812-8582, and the [‖‖]Department of Molecular Anatomy, Hamamatsu University School of Medicine, Shizuoka 431-3192, Japan

Neurons communicate with each other through synapses. To establish the precise yet flexible connections that make up neural networks in the brain, continuous synaptic modulation is required. The ubiquitin-proteasome system of protein degradation is one of the critical mechanisms that underlie this process, playing crucial roles in the regulation of synaptic structure and function. We identified a novel ubiquitin ligase, Fbxo45, that functions at synapses. Fbxo45 is evolutionarily conserved and selectively expressed in the nervous system. We demonstrated that the knockdown of Fbxo45 in primary cultured hippocampal neurons resulted in a greater frequency of miniature excitatory postsynaptic currents. We also found that Fbxo45 induces the degradation of a synaptic vesicle-priming factor, Munc13-1. We propose that Fbxo45 plays an important role in the regulation of neurotransmission by modulating Munc13-1 at the synapse.

The nervous system stores and retrieves information via synapses, which are its primary means of communication. Synapses are specialized intercellular junctions dedicated to the transfer of information from a neuron to another neuron. Synaptic transmission is rapidly, dynamically, efficiently, and tightly regulated by several molecular mechanisms (1–4). Among these mechanisms, recent studies have shown that synaptic components are modified by protein activation (5) and degradation (6–9).

Protein degradation can be mediated by the ubiquitin-proteasome system (UPS)[4] (10–12). The modification of proteins by the ligation of ubiquitin molecules is critical role in regulating the degradation of specific proteins, thereby controlling protein turnover. This control mechanism is extremely effective because it allows the rapid elimination of particular regulatory proteins, ensuring that the biological process regulated by the proteins can be shut down immediately. Protein ubiquitination is catalyzed by a cascade of reactions involving three enzymes: E1 (ubiquitin-activating enzyme), E2 (ubiquitin-conjugating enzyme), and E3 (ubiquitin-protein ligase). E1 activates ubiquitin in an ATP-dependent reaction and transfers it to E2 with the formation of a thiol ester bond between the C terminus of ubiquitin and a cysteine residue of E2. Next, E2, either by itself or together with E3, transfers the ubiquitin moiety to a lysine residue of the substrate protein. Various E3s have been reported, and the action of each is substrate-specific. Finally, the polyubiquitinated protein is attacked by the 26S proteasome complex, which rapidly degrades it into small fragments (13).

The E3s are presently categorized into four major classes based on their specific structural motif: HECT, RING finger, U-box, and PHD-finger types (14). The RING finger-type E3s are thought to be the largest family and are further divided into subfamilies; one of these, the cullin-based E3 subfamily, is one of the largest single classes of E3. There are seven cullin-based E3s, including the Skp1-Cul1-F-box-protein (SCF) complex and the anaphase-promoting complex/cyclosome (APC/C) (14). The SCF complex E3s are composed of the scaffold protein Cul1, the RING-domain protein Rbx1/Roc1, the adaptor pro-

* This work was supported by grants from Solution-oriented Research for Science and Technology, the Japan Science and Technology Agency, the Ministry of Education, Culture, Sports, Science, and Technology (MEXT) (to Hideyuki Okano) and by grants from Japan Society for the Promotion of Science, the Keio University grant-in-aid for Encouragement of Young Medical Scientists (to H. Tada), a grant-in-aid for Scientific Research on Priority Areas (to H. J. Okano), WAKATE S and SENTAN (to M. S.), and a grant-in-aid for the Global COE program (to Keio University) from the MEXT, Japan.

[S] The on-line version of this article (available at http://www.jbc.org) contains supplemental Figs. S1–S6.

[1] To whom correspondence may be addressed: Dept. of Physiology, Keio University School of Medicine, 35 Shinanomachi, Shinjuku-ku, Tokyo 160-8582, Japan. Tel.: 81-3-5363-3747; Fax: 81-3-3357-5445; E-mail: hjokano@sc.itc.keio.ac.jp.

[2] To whom correspondence may be addressed: Dept. of Molecular Anatomy, Hamamatsu University School of Medicine, 1-20-1 Handayama, Hamamatsu, Shizuoka 431-3192, Japan. Tel. and Fax: 81-53-435-2292; E-mail: setou@hama-med.ac.jp.

[3] To whom correspondence may be addressed: Dept. of Physiology, Keio University School of Medicine, 35 Shinanomachi, Shinjuku-ku, Tokyo 160-8582, Japan. Tel.: 81-3-5363-3747; Fax: 81-3-3357-5445; E-mail: hidokano@sc.itc.keio.ac.jp.

[4] The abbreviations used are: UPS, ubiquitin-proteasome system; SCF , Skp1-Cul1-F-box-protein; PBS, phosphate-buffered saline; GFP, green fluorescent protein; DIV, days *in vitro*; siRNA, short interfering RNA; aa, amino acids; PSD, postsynaptic density; mEPSC, miniature excitatory postsynaptic current; EGFP, enhanced green fluorescent protein; HA, hemagglutinin.

tein Skp1, and one of many F-box proteins, which function to bind the substrate and constitute the largest known class of E3-specificity components. Rbx1 associates with Cul1 and E2, whereas Skp1 interacts with Cul1 and the F-box protein. The F-box protein interacts with Skp1 via its F-box motif and with substrates via its C-terminal protein-protein interaction domain (15, 16). Target molecules of several F-box proteins have been reported; for example, β-TrCP, an F-box protein that contains WD40 domain repeats, was identified as the intracellular receptor in SCF E3 for β-catenin and IκBα (17, 18); Skp2, which recognizes cyclin-dependent kinase inhibitors such as $p27^{Kip1}$, $p21^{Cip1}$, and $p57^{Kip2}$, is an F-box protein containing seven leucine-rich repeats (19).

The UPS in synaptic sites plays various roles throughout the life cycle of the synapse, *i.e.* in synaptic development, maintenance, and plasticity (6). Genetic studies in *Drosophila* and *Caenorhabditis elegans* have demonstrated the importance of E3s in synaptic development and function. For example, mutations of *highwire*, a putative E3 in *Drosophila*, or of its orthologue in *C. elegans* (*rpm-1*) lead to aberrant synaptic development (20–23). Moreover, recent studies have identified several additional mammalian E3s at the synaptic site, including SCRAPPER (9), Siah (24, 25), Staring (26), and Parkin (27). Although ample evidence supports the role of protein ubiquitination in synaptic development and plasticity in vertebrates (28), the specific molecular mechanisms underlying these effects remain to be elucidated.

Here we identified a novel synaptic E3, Fbxo45, by expression screening using the autoimmune antiserum from a patient with stomach cancer associated with psychiatric symptoms. To examine E3 functions at the synapse with potential relevance to neuronal disease, we recorded the miniature excitatory postsynaptic current (mEPSC) in hippocampal neuronal culture with or without Fbxo45. We demonstrated that Fbxo45 regulates neurotransmission at mature neurons and provides evidence that Munc13-1 may be a target or downstream molecule through which Fbxo45 acts in synaptic transmission.

EXPERIMENTAL PROCEDURES

Patient Serum and Cerebrospinal Fluid—A gastric cancer (Borrmann iv) patient showed psychiatric symptoms including severe depression, involutional melancholia, and amnesia and had high titer autoantibodies in the serum and cerebrospinal fluid, typically observed in patients with paraneoplastic neurologic disorder, a rare neurologic disorder caused by the remote effects of cancer that is thought to be immune-mediated (29, 30). Samples of the patient's serum (5 ml) and cerebrospinal fluid (3 ml) were collected. The serum and cerebrospinal fluid were spun at 15,000 × *g* for 15 min, and the supernatants were used in the following studies. All of the experimental procedures were performed with the approval of the Ethical Committee of Keio University School of Medicine.

Expression Screening—A λZAP mouse brain expression cDNA library was screened at a density of 4.5×10^5 plaque-forming units/225-mm plates. After 2 h of incubation at 42 °C, the plates were overlaid with filters soaked in 10 mM isopropyl β D-thiogalactopyranoside and incubated for 16 h at 37 °C. The plates were then cooled for 1 h at 4 °C, and the filters were removed, blocked with blocking buffer (5% skim milk and 0.5% bovine serum albumin) for 1 h, and incubated for 3 h with the patient's serum (1:500). After being washed 5 times for 6 min in washing buffer (Tris-buffered saline containing 1% Tween 20 (TBST)), the filters were incubated with horseradish peroxidase-conjugated anti-human IgG secondary antibodies (1:5000) for 1 h, and the immunoreactivities were detected using the ECL system (Amersham Biosciences).

Positive clones were purified by several rounds of antibody screening until a yield of 100% positive plaques was obtained. Phage clones were subcloned in a pBK-CMV phagemid vector using the *in vivo* excision phage rescue protocol (Stratagene).

In Situ Hybridization—Sense and antisense RNA probes (858 bp) for mouse *Fbxo45* were transcribed *in vitro* by T7 or SP6 RNA polymerase with digoxigenin-labeled UTP (Roche Applied Science). Mice were anesthetized, and the whole brain was removed. Serial frozen mouse sections (14 μm) were incubated overnight at 55 °C in a moist chamber with 200 μg of the sense or antisense probe per 50 μl of a buffer containing 50% formamide, 5× SSC (1× SSC = 0.15 M NaCl and 0.015 M sodium citrate), 50 μg/ml *Escherichia coli* tRNA, 50 μg/ml heparin sodium, and 1% SDS. The specimens were washed in 50% formamide, 5× SSC (30 min at 55 °C), 2× SSC (3 times for 30 min at 55 °C), and TBST (twice for 20 min at room temperature). After being blocked in 0.5% bovine serum albumin in TBST (60 min), the slides were incubated with an alkaline phosphatase-conjugated anti- digoxigenin antibody (Roche Applied Science) in the above buffer (overnight at 4 °C), then washed in TBST (3 times for 20 min) and NTM (100 mM NaCl, 50 mM $MgCl_2$, and 100 mM Tris-HCl, pH 9.5) for 10 min. Signals were detected in NTM containing 450 μg/ml 4-nitroblue tetrazolium chloride and 175 μg/ml 5-bromo-4-chloro-3-indolylphosphate according to the digoxigenin RNA detection kit (Roche Applied Science).

Northern Blot Analysis—Total RNAs (20 μg) from embryonic and postnatal brain and from adult mouse tissues were prepared with TRIzol reagent (Invitrogen) following the manufacturer's protocol. Purified RNAs were loaded onto a 1% formaldehyde-agarose gel after being denatured at 70 °C for 10 min. The RNAs were transferred to a nylon membrane (Amersham Biosciences) and UV-cross-linked using a Stratalinker (Stratagene). The membrane was hybridized at 51 °C with a full-length mouse *Fbxo45* or glyceraldehyde-3-phosphate dehydrogenase (*G3PDH*) cDNA probe that had been labeled with [α-^{32}P]dCTP using a Prime-It labeling kit (Stratagene). The blots were washed at 65 °C in 2, 1, and then 0.1% standard sodium citrate containing 0.1% SDS and were exposed to MR film (Eastman Kodak Co.).

Antibodies—The following antibodies were used: Synapsin-I, Munc13-1 (Synaptic Systems), synaptophysin, β-actin, FLAG, and Myc (Sigma), GFP (Wako), PSD-95 and Myc (Upstate Biotechnology), VGlut1 (Chemicon), PSD-95 (Cell Signaling), pan-Munc13, synaptotagmin, SNAP25, synaptogyrin, and Skp1 (BD Biosciences), and GFP and hemagglutinin (HA) (MBL).

To produce an anti-Fbxo45 polyclonal antibody, glutathione *S*-transferase-tagged full-length Fbxo45 (for immunohistochemistry, immunocytochemistry, and immuno-electron microscopy) or C- (257–286) terminal Fbxo45 (for immuno-

blot) bacterial fusion proteins were purified and dialyzed against PBS as described above. Rabbits were given injections of 2.5 mg of a mixture of the proteins at 3-week intervals. The antibodies were obtained by passing the serum through a column containing glutathione *S*-transferase fusion versions of the proteins.

Plasmid Construction—GFP-tagged Fbxo45 was inserted into a pEGFP-C1 vector (Clontech), and FLAG-tagged Fbxo45 and Fbxo45 deletion mutants (1–140, 54–140, and 101–286 aa) were inserted into a pFLAG-CMV-2 vector (Eastman Kodak Co.) or p3xFLAG-CMV-7.1 vector (Sigma). FLAG-Msi1, FLAG-HuC, Myc-Skp1, Myc-Munc13-1, Myc-RIM1, and HA-ubiquitin were prepared as described previously (9, 31–34, 55).

Immunoelectron Microscopy—For immunoelectron microscopic analysis, frozen sections were incubated with the anti-Fbxo45 primary antibody (1:500) followed by incubation with a nanogold-conjugated anti-rabbit secondary antibody (1:100; Invitrogen). After glutaraldehyde fixation, the signals were enhanced by a 10-min HQ-Silver kit reaction (Nanoprobes Inc.). The sections were postfixed with 0.5% osmium tetroxide, dehydrated through ethanol, and embedded in Epon. Ultrathin sections (70 μm) were cut and stained with uranyl acetate and lead citrate, observed under a transmission electron microscopy (JEOL model 1230), and photographed with a Digital Micrograph 3.3 (Gatan Inc.). For quantitative analysis, nanogold density was calculated in each neuronal compartment by counting the number of nanogold particles in every immunoelectron microscopic images using MetaMorph software (Molecular Devices, Toronto, Canada). The mean number of nanogold particles and the mean area of each compartment was measured for all discernible structures of synapse and myelin from three independent immunoelectron microscopic experiments (35).

Immunocytochemistry and Image Analysis—The cultured hippocampal neurons were prepared as described previously (9, 36). Cultured cells were fixed with 4% paraformaldehyde in PBS for 30 min at day *in vitro* (DIV) 17–18. The cells were permeabilized with 0.2% Triton X-100 for 10 min, washed with PBS, and then incubated in PBS containing TNB (PerkinElmer Life Sciences) for 1 h. The preparation was then incubated with Fbxo45 (1:100), VGlut1 (1:5000), anti-Synapsin-I (1:1000), and anti-PSD-95 (1:100) antibodies overnight at 4 °C, and after extensive washes with PBS, the preparation was overlaid with secondary antibody solution for 1 h at room temperature.

Image acquisition was performed using an LSM 510 (Carl Zeiss) and FluoView 1000 (Olympus) confocal microscope. The clusters of Synapsin-I (red)/PSD-95 (white) colocalization were counted. The red and white images were merged, the colocalized signals over the dendrites of GFP-expressing neurons were determined, and the values were entered into Microsoft Excel. The transfected neurons were chosen randomly from three independent experiments for each construct. All experiments on live animals were performed in accordance with Keio University guidelines and regulations.

Recording of the mEPSC—Cultured cells were transfected using the Lipofectamine 2000 reagent (Invitrogen) 3 days before electrophysiological analysis. For the mEPSC recording, the culture medium was replaced with a saline solution containing 168 mM NaCl, 2.4 mM KCl, 2, 5, or 10 mM $CaCl_2$, 1 mM $MgCl_2$, 10 mM glucose, 10 mM HEPES, and 0.5 μM tetrodotoxin, pH 7.3. The electrodes (5–8 MΩ) were filled with whole-cell pipette solution containing 120 mM potassium acetate, 20 mM KCl, 0.1 mM $CaCl_2$, 5 mM $MgCl_2$, 0.2 mM EGTA, 5 mM ATP, and 10 mM HEPES, pH 7.3. The whole-cell recording of GFP-expressing neurons was configured using an EPC-7 amplifier (HEKA) and a Digidata 1200 acquisition board (Axon Instruments). The membrane potential was clamped at 60 mV, and the signals were filtered at 10 kHz with the gain set at 0.5 mV/pA for 40-s recording periods. In all instances cells were excluded from analysis if a leak current >300 pA was observed. Membrane resistance (*R*m), series resistance (*R*s), and membrane capacitance (*C*m) were monitored. Only recordings with $Rm > 100$ MΩ and $Rs < 20$ MΩ were included for analysis. The mean *R*m, *R*s, and *C*m were not different ($p > 0.05$) among or within groups of cells being compared. Measurements of the frequency and amplitude of mEPSC were acquired for a period of 40 s. The mEPSC was detected by setting the amplitude threshold to the background noise level ×3 (in all electrophysiological experiments, a similar amount of data from GFP-expressing neurons transfected with each construct was acquired on the same day). The data from each neuron were then averaged and tested for statistical significance. All electrophysiological experiments were performed from at least three different platings of neurons for each of three different transfections. See our previously published method for details (5).

RNA Interference—Short interfering RNA (siRNA) duplexes for Fbxo45 were: siRNA Fbxo45-1, sense (5′-GGACCAAGAUUGGUUUCAGtt-3′) and antisense (5′-CUGAAACCAAUCUUGGUCCtt-3′); siRNA Fbxo45-2, sense (5′-GGUUUUACAUUACAUCGGAtt-3′) and antisense (5′-UCCGAUGUAAUGUAAAACCat-3′). The recommended negative control were obtained from Ambion in annealed and purified forms. Transfection of the siRNA duplexes was carried out using Lipofectamine 2000 (Invitrogen). Three microliters of Lipofectamine 2000 reagent with 100 pmol of siRNA duplex and 0.5 μg of pEGFP were transfected into cultured hippocampal neurons at DIV14. Three days after transfection, the cells were subjected to mEPSC recording.

Transfection, Immunoprecipitation, and Ubiquitination Assay—293T cells or COS cells were transfected using the FuGENE transfection reagent (Roche Applied Science) and harvested 48 h later. For the ubiquitination assay, the cells were treated with 50 μg/ml MG132 (Peptide Institute) for 3 h before they were harvested. Immunoprecipitates prepared with anti-FLAG M2 affinity gel or anti-c-Myc-agarose conjugate (Sigma) were used for immunoblotting with the appropriate antibodies.

Miscellaneous Procedures—Immunoblotting analyses were performed as described (37). The subcellular fractionation analysis of mouse brain extract was performed as described (38, 39). The stability of Munc13-1 was determined by treatment with 50 mg/ml cycloheximide (Calbiochem) for the indicated times.

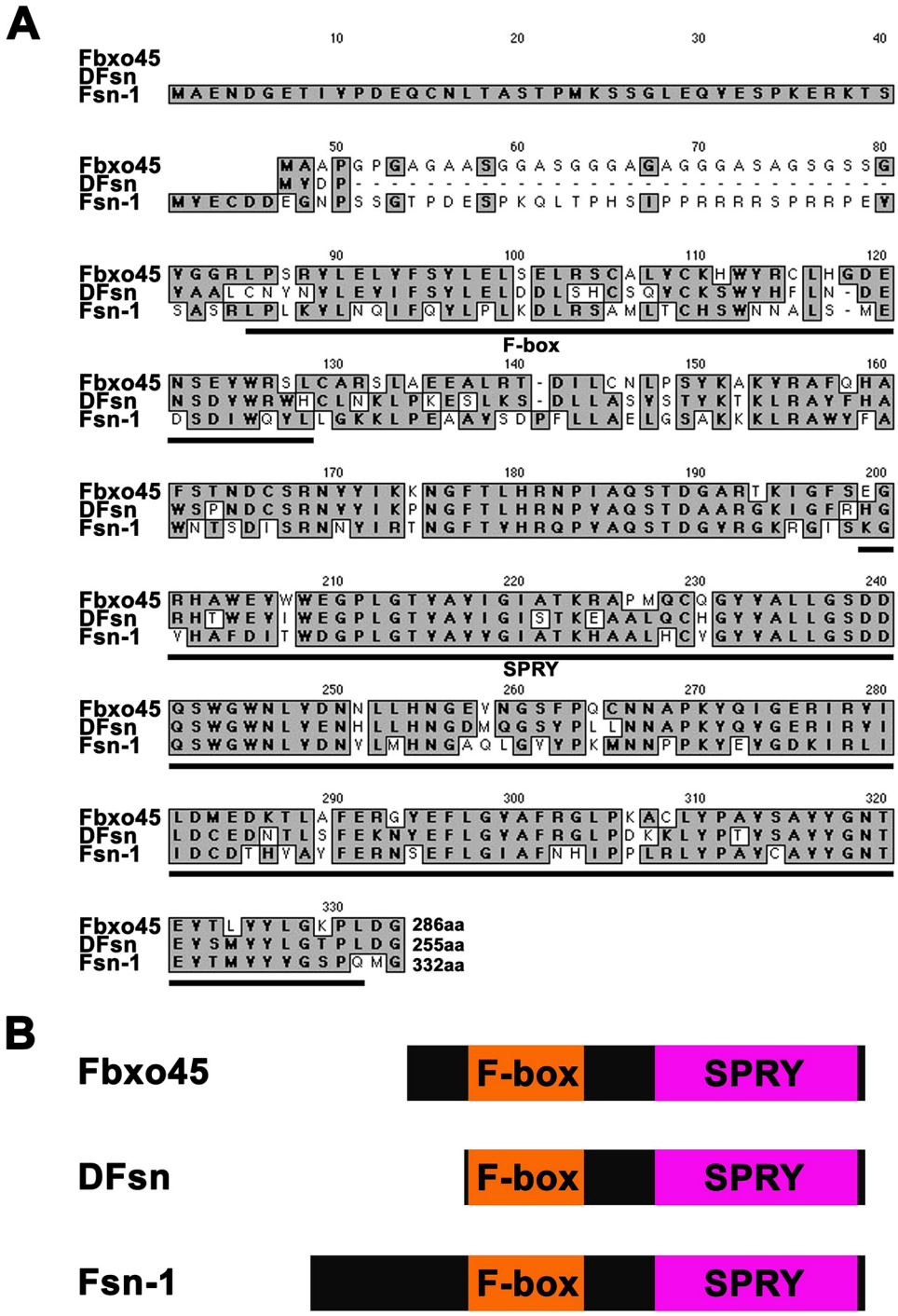

FIGURE 1. **Identification of a novel F-box protein, Fbxo45.** *A*, the amino acid sequence of mouse Fbxo45 compared with its *Drosophila* (*DFsn*) and *C. elegans* (*FSN-1*) homologues is shown. The conserved amino acids are *highlighted* in *gray*. The *underlines* indicate the signature sequences of the F-box and SPRY domains. *B*, domain structures of Fbxo45, DFsn, and FSN-1.

The *Fbxo45* gene was located on chromosome 16 in *Mus musculus* and encoded a 286-amino acid protein with an estimated molecular mass of 30 kDa. Data base (National Center for Biotechnology Information) searches with the deduced amino acid sequence of Fbxo45 revealed that it was a novel protein with striking similarity (99% identity) to a *Homo sapiens* F-box protein encoded by a gene located on chromosome 3. Recently, mammalian F-box proteins were systematically classified, and the protein corresponding to Fbxo45 was named FBXO45 (40, 41). The amino acid sequence of the Fbxo45 protein was highly conserved among species, including *Drosophila* DFsn/CG4643-PA; isoform A, CG4643-PB; isoform B (GenBank^{TM} accession no. NP_610849, NP_725266), and *C. elegans* FSN-1 (GenBank^{TM} accession no. NP_498046) (Fig. 1).

The deduced Fbxo45 amino acid sequence displayed some notable primary structural characteristics: an F-box domain of ~45 amino acids, located in its N-terminal region, and a SPRY (SPla and the ryanodine receptor) domain, the function of which remains unknown (42). F-box motifs are found in proteins that function as the substrate recognition component of SCF E3 complexes. The patient's autoantibodies in the serum and cerebrospinal fluid recognized the F-box domain in Fbxo45 (supplemental Fig. S1).

Tissue Distribution of Fbxo45—To elucidate the expression pattern of *Fbxo45* mRNA, we performed Northern blots, immunoblotting analyses, and *in situ* hybridization on mouse tissue preparations. The *Fbxo45* mRNA, which was ~2.7 kb, was detected preferentially in the brain at similar levels throughout development, from E12 to adulthood, and was undetectable in the tissues outside the nervous system (Fig. 2*A*). We next raised a Fbxo45-specific polyclonal antibody that recognized the 30-kDa endogenous Fbxo45 protein. Immunoblot analysis of mouse brain tissues revealed that Fbxo45 was expressed widely in the central nervous system, including the olfactory bulb, hippocampus, cortex, cerebellum, and brain stem (Fig. 3*A*, supplemental Fig. S3). *In situ* hybridization analysis showed that the

RESULTS

Identification of a Novel F-box Protein, Fbxo45—To identify the target molecule recognized by the autoantibody of a cancer patient with psychiatric symptoms, we performed expression screening of a mouse brain cDNA library using the patient's serum. From 1×10^6 clones screened, four positive clones were isolated. Sequence analysis showed that all four clones encoded overlapping sequences of the same cDNA, *Fbxo45*.

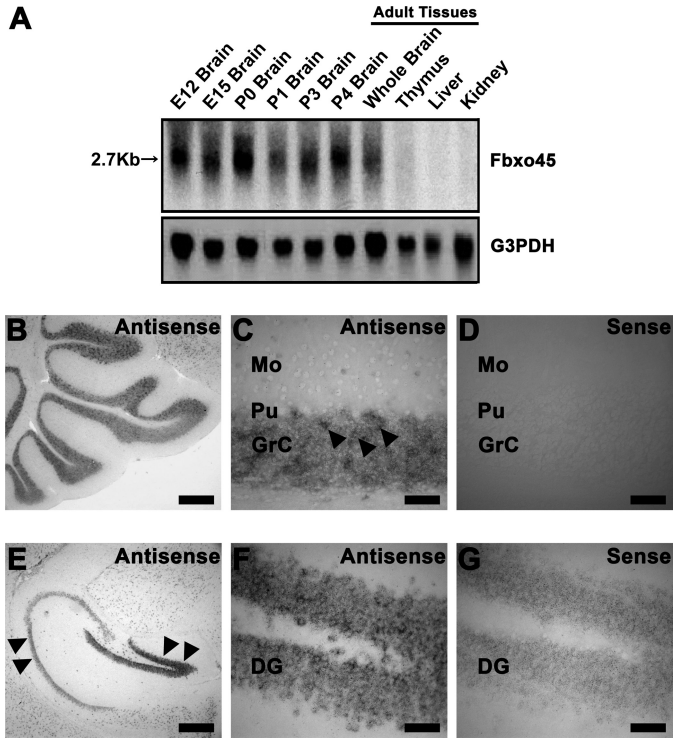

FIGURE 2. **Fbxo45 mRNA expression.** *A*, shown is a Northern blot analysis of *Fbxo45* mRNA in embryonic brain and adult tissues from mice. *G3PDH*, glyceraldehyde-3-phosphate dehydrogenase. *B–G*, shown is an *in situ* hybridization analysis of *Fbxo45* in the brain. Sagittal sections of adult mouse brain were hybridized with an antisense or sense *Fbxo45*-specific cRNA probe. *Fbxo45* expression was observed in the cerebellum (*B–D*) and hippocampus (*E–G*) as indicated by *arrowheads*. No signal was detected with the sense probe (*D* and *G*). *Mo*, Molecular layer; *Pu*, Purkinje cell layer; *GrC*, granule cell layer; *DG*, dentate gyrus. *Scale bars*: 400 μm in *B* and *E*, 50 μm in *C*, *D*, *F*, and *G*.

Fbxo45 mRNA was highly expressed in the granule cell layer of the cerebellum, dentate gyrus of the hippocampus (Fig. 2, *B–G*), granule cell layer of the olfactory bulb, and subventricular zone of the lateral ventricle (supplemental Fig. S2, *A* and *B*). It was also expressed in some cells in the cortex (supplemental Fig. S2*C*).

Expression of Fbxo45 in the Nervous System—To determine the precise location of the Fbxo45 protein in the nervous system, we examined the subcellular distribution of Fbxo45 by subcellular fractionation. Fbxo45 was enriched in the synaptic fractions, which included the synaptosomal membrane fraction (LP1), synaptic plasma membrane fraction (*SPM*), and the postsynaptic density (*PSD*) fraction (Fig. 3*B*).

We also performed immunohistochemistry using the anti-Fbxo45 polyclonal antibody, whose immunoreactivity disappeared in Fbxo45 knock-out mice (supplemental Fig. S4). Endogenous Fbxo45 protein was detected as a spotty and fibrous pattern in the primary cultured rat hippocampal neuron at DIV 16 (Fig. 3*C*). The Fbxo45 immunoreactivity was colocalized in part with a presynaptic marker, VGlut1, and a postsynaptic marker, PSD-95. Analyses using immunoelectron microscopy revealed that the significantly higher expression of Fbxo45 in both pre- and postsynaptic structures of excitatory neuron was detected compared with that in myelin cytoplasm (Fig. 3, *D* and *E*, supplemental Fig. S6). Taken together, these results support the idea that Fbxo45 could have a physiological function at the synapse.

Involvement of Fbxo45 in Neurotransmission in Rat Hippocampal Neurons—Because FSN-1, the Fbxo45 homologue in *C. elegans,* is involved in aspects of synapse formation such as the clustering of periactive zones (43), we investigated Fbxo45 involvement in synaptic function. First, we immunostained primary cultured hippocampal neurons at DIV 14 transfected with an expression vector bearing FLAG-tagged full-length Fbxo45 (FLAG-Fbxo45), vector control (FLAG-Vec), Fbxo45 siRNAs (siRNA Fbxo45-1 and -2), which significantly decreased the level of endogenous Fbxo45 protein (supplemental Fig. S5), or siRNA control (*siRNA Cont.*) for Synapsin-I and PSD-95 (Fig. 4*A*) as a marker for synapses and then evaluated whether the expression of Fbxo45 altered the number of the synapses, defined as sites in which Synapsin-I and PSD-95 were colocalized. A quantitative analysis showed no significant change in the synaptic number (Fig. 4*B*), indicating that Fbxo45 did not influence synapse formation in mature neurons.

Next, we recorded the mEPSC under whole-cell voltage clamp after blocking the sodium channel-mediated action potential activity with tetrodotoxin. Primary cultured rat hippocampal neurons at DIV 14 were transfected with Fbxo45, Fbxo45 deletion mutants (54–140 or 101–286 aa), vector control, siRNA Fbxo45-1 and -2, or siRNA control along with an EGFP-bearing vector, and the mEPSC was recorded 3 days later. We found that the knockdown of Fbxo45 significantly increased the mEPSC frequency without changing its amplitude. In contrast, the overexpression of Fbxo45 decreased the mEPSC frequency. Furthermore, a dominant-negative deletion mutant Fbxo45 (101–286 aa) lacking its F-box domain increased the mEPSC as did the siRNAs (Fig. 4, *C* and *D*). The frequency of the mEPSC was increased or decreased by the change of Fbxo45 protein level with an extracellular Ca^{2+} concentration of 2 mM; however, there was no significant difference in the mEPSC frequency compared with the control at a higher extracellular Ca^{2+} concentration (10 mM) (Fig. 4*E*). These results show that Fbxo45 functions as a negative regulator of mEPSC frequency in an extracellular Ca^{2+} concentration-dependent manner. Because Fbxo45 did not alter synapse formation in mature neurons, these findings strongly suggest that Fbxo45 regulates neurotransmission machinery.

Fbxo45 Interacts with Skp1 and Induces Protein Ubiquitination—It is known that the F-box proteins interact with an adaptor protein Skp1 and constitute the larger class of E3 specificity components. To evaluate whether Fbxo45 interacts with Skp1, we performed co-immunoprecipitation analyses. FLAG-Fbxo45, FLAG-Musashi1 (FLAG-Msi1) (31, 44), or FLAG-HuC were overexpressed in 293T cells and immunoprecipitated with a monoclonal antibody against the FLAG epitope. In the result, endogenous Skp1 was co-immunoprecipitated with overexpressed FLAG-Fbxo45 (Fig. 5*A*). The structure of Fbxo45 to form SCF complex has been described elsewhere (45).

To clarify the relationship between Fbxo45 and the ubiquitin proteolytic system, we examined whether Fbxo45 traps target proteins for the ultimate ubiquitination. Immunoblots showed multiple ubiquitinated bands of high molecular mass in the anti-FLAG immunoprecipitates from 293T cells co-transfected with FLAG-Fbxo45 and HA-tagged ubiquitin after pretreatment with the proteasome inhibitor MG132. In contrast, no

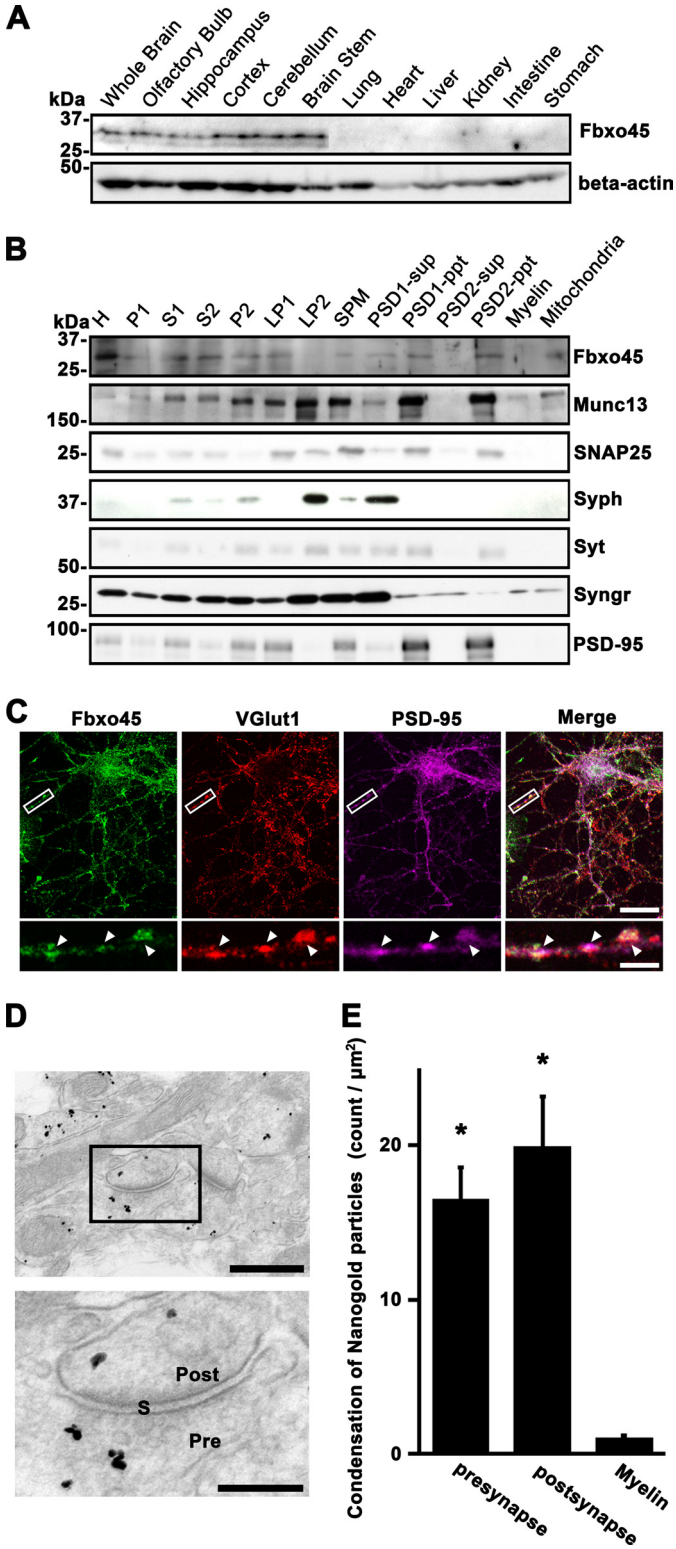

FIGURE 3. **Fbxo45 protein expression.** *A*, immunoblot analysis of Fbxo45 in adult mice is shown. *B*, subcellular distribution of Fbxo45 in the mouse brain is shown. Immunoblot analysis of Fbxo45, Munc13, SNAP25, synaptophysin (*Syph*), synaptotagmin (*Syt*), synaptogyrin (*Syngr*), or PSD-95 in the indicated fractions showed that Fbxo45 was enriched at the synaptic region, including the synaptosomal membrane fraction (*LP1*) and postsynaptic density (*PSD*). *H*, homogenate; *P1*, nuclear fraction; *S1*, crude synaptosomal fraction; *S2*, cytosolic synaptosomal fraction; *P2*, crude synaptosomal pellet fraction; *LP2*, synaptosomal vesicle fraction; *SPM*, synaptic plasma membrane fraction. *C*, immunocytochemistry of primary cultured rat hippocampal neurons expressing Fbxo45 is shown. Shown are Fbxo45 (*green*), VGlut1 (*red*), and PSD-95 (*purple*) (*upper panels*). Magnifications of the *boxed areas* in the *upper panels* are shown in the *lower panels*. *Arrowheads* indicate synapses, at which VGlut1 and PSD-95 were colocalized. *Scale bars*: 20 μm in the *upper panels*, 5 μm in the *lower panels*). *D*, shown is immunoelectron microscopy of endogenous Fbxo45. The *lower panel* shows a magnified image of the *boxed area* in the *upper panel*. *S*, synapse; *Pre*, presynaptic terminal; *Post*, postsynaptic terminal. *Scale bars*: 0.5 μm in the *upper panel*, 0.2 μm in the *lower panel*. *E*, localization of nanogold particles was quantitatively evaluated on each indicated structures (count/μm²). *Asterisk*, unpaired *t* test, $p < 0.01$.

ubiquitinated bands were detected in immunoprecipitates prepared from cells without FLAG-Fbxo45 (Fig. 5*B*). These results indicate that Fbxo45 indeed induced the ubiquitination.

Involvement of Fbxo45 in the Degradation of Munc13-1—The findings that Fbxo45 regulates mEPSC frequency and protein ubiquitination led us to speculate that Fbxo45 might control the degradation of a substrate in the nerve terminal to regulate neurotransmission. To find candidate substrates of Fbxo45, we first evaluated several synaptic proteins immunoprecipitated with Fbxo45. Munc13-1, the synaptic vesicle priming factor, was identified as one of Fbxo45-binding proteins. Moreover, we found that Munc13-1 interacted with the Fbxo45 deletion mutant (101–286 aa) that included the SPRY domain but not with deletion mutants lacking the SPRY domain (54–140 and 1–140 aa) (Fig. 6*A*).

To examine whether Fbxo45 affects the protein level of Munc13-1, we first co-expressed FLAG-Fbxo45 and Myc-Munc13-1 or Myc-RIM1 (rab3-interacting molecule 1), another vesicle priming factor in COS cells. With the expression of Fbxo45, the level of Munc13-1 decreased in a dose-dependent manner, but in sharp contrast the level of RIM1 did not change (Fig. 6*B*).

Next, to examine whether Fbxo45 affects the stability of Munc13-1, we co-transfected 293T cells with Munc13-1, Fbxo45, and Fbxo45 deletion mutants and then inhibited new protein synthesis by incubating the cells with cycloheximide for various times. The stability of Munc13-1 was assessed by immunoblotting analysis. The overexpression of Fbxo45 promoted a significantly faster degradation of Munc13-1 (half-life 4 h) compared with the control (Vec, Fbxo45 deletion mutants). In contrast, degradation of Munc13-1 was inhibited and rebuilt to control the level in Fbxo45-expressing cells treated with MG132 (Fig. 6*C*). The knockdown of Fbxo45 also showed delay of degradation of endogenous Munc13-1 (Fig. 6*D*). These results indicate that Fbxo45 interacts with Munc13-1 via SPRY domain and leads to degradation by UPS.

DISCUSSION

Information is passed from one neuron to the next by the release of neurotransmitters at the synapse. Neurotransmitter release is mediated by recycled neurotransmitter-containing synaptic vesicles at the presynaptic plasma membrane. A key event in neurotransmitter release is the priming step, which takes place before the fusion of a synaptic vesicle with the presynaptic active zone membrane. The priming step dramatically increases the propensity for vesicular release by lowering the energy barrier for fusion, thereby enabling the vesicles to use the action potential-induced transient Ca^{2+} increase efficiently for rapid exocytosis (46). Munc13-1 plays an essential role in

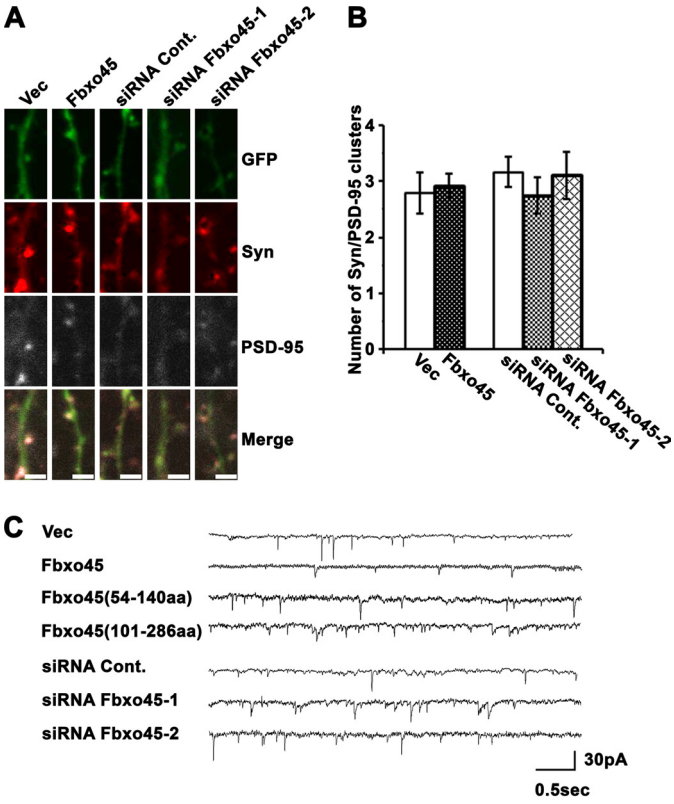

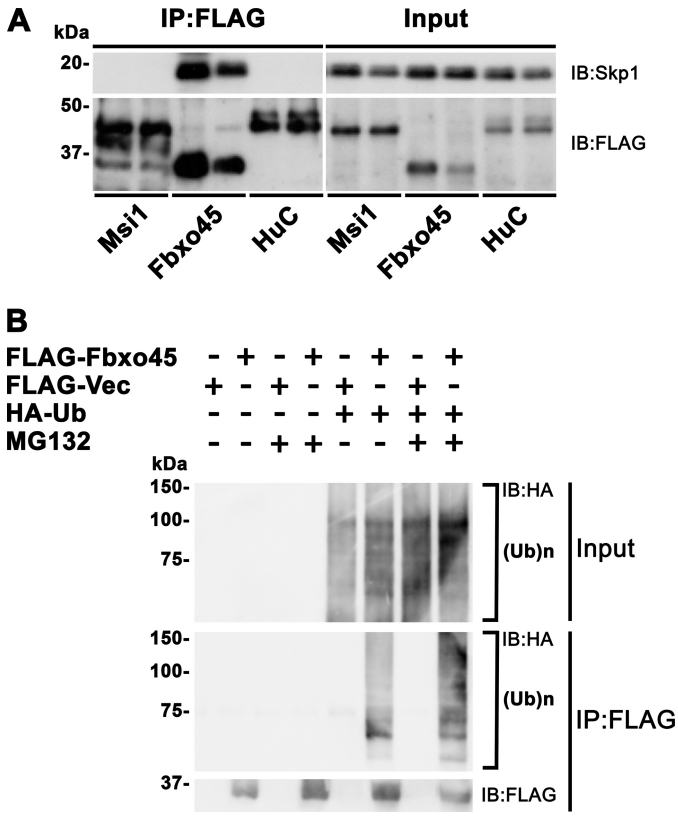

FIGURE 5. **Fbxo45 interacts with Skp1 and induces protein ubiquitination.** *A*, shown is an immunoprecipitation (*IP*) assay of FLAG-Fbxo45 with endogenous Skp1 compared with FLAG-Musashi1 (Msi1) or FLAG-HuC as a negative control. *IB*, immunoblot. *B*, shown is ubiquitination activity of Fbxo45 in 293T cells. The high molecular mass, ubiquitinated proteins are labeled *(Ub)n* at the *right*.

the neurotransmitter release machinery. In Munc13-1-deficient neurons, both spontaneous and evoked transmitter secretion are dramatically reduced, while vesicle docking to the active zone is essentially normal (47–50). On the other hand, the overexpression of Munc13-1 enhances neurotransmitter release at neuromuscular junctions in *Xenopus* (51). To control the level of Munc13-1 protein at synaptic sites, a spatially regulated protein degradation system like UPS is required. In support of this concept, the *Drosophila* Munc13-1 homologue DUNC13 is ubiquitinated, and it selectively accumulates in the

FIGURE 4. **Regulation of synaptic activity by Fbxo45.** *A*, shown is immunocytochemistry of cultured hippocampal neurons transfected with full-length of Fbxo45, vector control (*Vec*), siRNAs against Fbxo45 (*siRNA Fbxo45-1*, *siRNA Fbxo45-2*), or a control siRNA (*siRNA Cont.*) and EGFP. GFP (*green*), Synapsin-I (*Syn*; *red*), and PSD-95 (*white*) (scale *bars*: 5 μm). *B*, shown is quantification of the clusters that Synapsin-I and PSD-95 colocalized in the dendrites shown in *A*. *Vec*, $n = 18$; *Fbxo45*, $n = 29$; *siRNA control*, $n = 24$; siRNA Fbxo45-1, $n = 20$; *siRNA Fbxo45-2*, $n = 11$ dendrites. *C*, shown is a representative recording of the α-amino-3-hydroxy-5-methyl-4-isoxazolepropionate receptor-mediated mEPSC from neurons transfected with full-length or deletion mutants of Fbxo45, vector control, siRNAs against Fbxo45, or a control siRNA. *D*, quantification is shown of the mEPSC frequency and amplitude under the conditions described in *C*. *Vec*, $n = 11$; *Fbxo45*, $n = 9$; *Fbxo45(54–140aa)*, $n = 9$; *Fbxo45(101–286aa)*, $n = 9$; *siRNA control*, $n = 9$; *siRNA Fbxo45-1*, $n = 12$; *siRNA Fbxo45-2*, $n = 6$ neurons; *asterisk*, unpaired *t* test, $p < 0.05$). *E*, shown is mEPSC frequency in neurons transfected with Fbxo45 or the control vector in 2, 5, or 10 mM extracellular Ca^{2+}. (*Vec*, $n = 11, 14, 14$; *Fbxo45*, $n = 12, 8, 13$; *siRNA control*, $n = 9, 6, 7$; *siRNA Fbxo45-1*, $n = 12, 9, 8$; *siRNA Fbxo45-2*, $n = 6, 6, 7$ neurons (2, 5, 10 mM extracellular Ca^{2+}); *asterisk*, unpaired *t* test, $p < 0.05$.

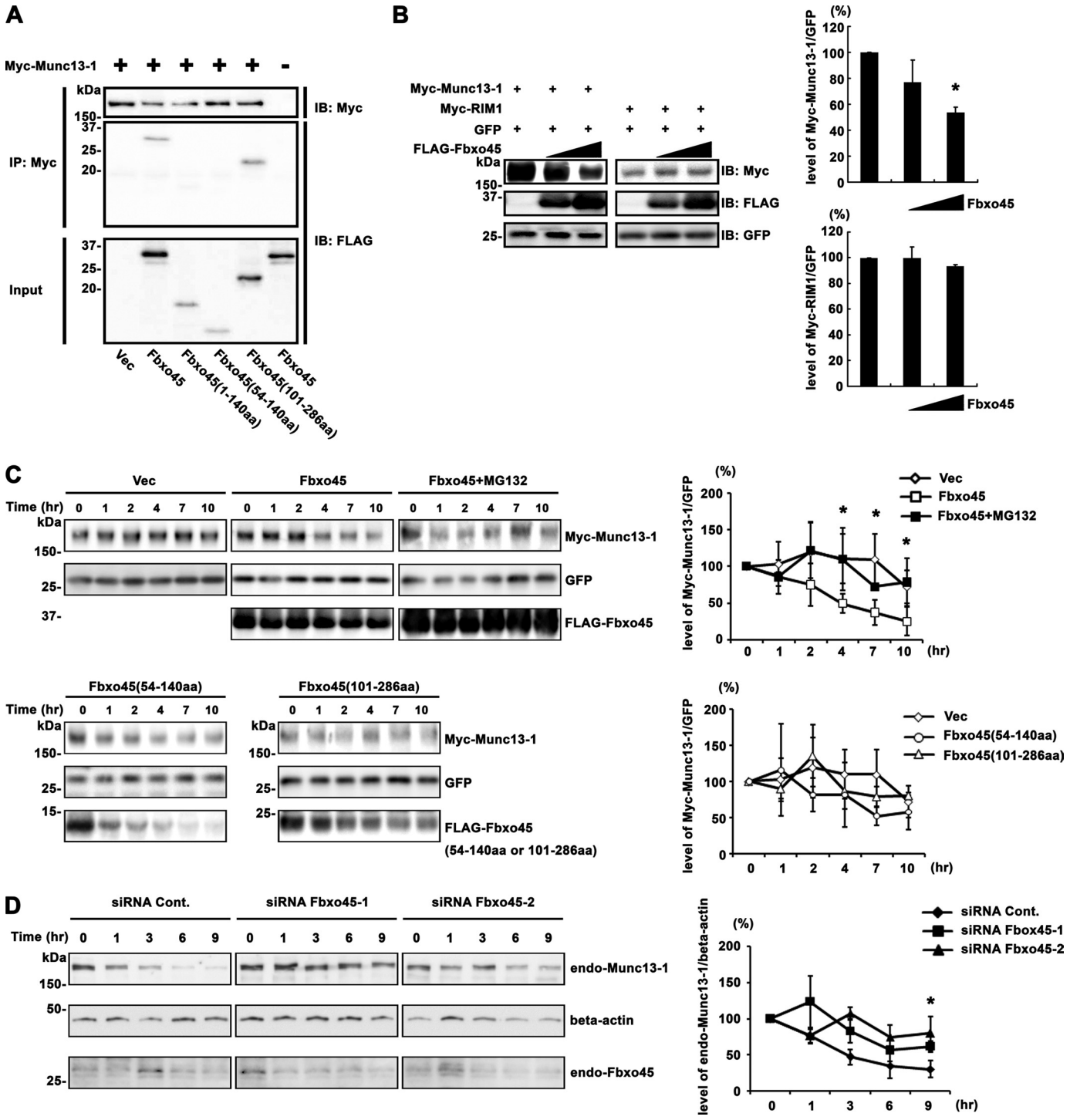

FIGURE 6. **Involvement of Fbxo45 in the degradation of Munc13-1.** *A*, Fbxo45 interacts with Munc13-1 through the SPRY domain. FLAG-tagged full-length or deletion mutants of Fbxo45 were co-expressed with Myc-Munc13-1 in 293T cells and then immunoprecipitated (*IP*) with an anti-Myc antibody. The precipitates were analyzed by immunoblotting (*IB*) using an anti-FLAG or anti-Myc antibody. *Vec*, vector. *B*, the level of Munc13-1 protein was decreased by Fbxo45 in a dose-dependent manner. In contrast, the RIM1 level was not affected by Fbxo45. Shown is quantification of the optical densities of the Munc13-1 and RIM1 bands. The protein levels, normalized to those of the corresponding EGFP bands, are shown as a percentage of the normalized value without Fbxo45 co-expression. *Asterisk*, $p < 0.05$, Mann-Whitney *U* test. *C*, shown is regulation of Munc13-1 stability by Fbxo45. Munc13-1 was co-expressed with Fbxo45 full-length, Fbxo45 deletion mutants, or Fbxo45 with MG132 and EGFP in 293T cells. *D*, shown is regulation of endogenous Munc13-1 protein stability by endogenous Fbxo45 in Neuro2A cells. siRNA control or siRNAs against Fbxo45 were transfected into Neuro2A cell. The protein stability was assessed by immunoblot analysis after incubation with cycloheximide for various times. Protein decay curves were determined from these studies. The optical density of the Munc13-1 or endogenous Munc13-1 bands was normalized to that of the corresponding EGFP or β-actin band, respectively, and is shown as a percentage of the normalized value for the 0-h time point. *Asterisk*, $p < 0.05$. Mann-Whitney *U* test.

presynaptic terminal after proteasome inhibition (52), although the E3 for DUNC13 is still unknown.

In the present study we cloned and identified the *Fbxo45* gene, which encodes an F-box ubiquitin ligase that is specifically expressed in the nervous system. Our newly generated anti-Fbxo45 antibody demonstrated the synaptic localization of Fbxo45. Subcellular distribution assay showed that Fbxo45 expression overlapped with presynaptic protein Munc13 in LP1, synaptic plasma membrane fraction, and PSD. Fbxo45 functions as a ubiquitin ligase of vesicle-priming factor Munc13-1 and regulated the spontaneous mEPSC activity in mature neurons. Munc13-1-deficient mice have been shown to exhibit a decrease of mEPSC frequency (53), which was almost same quantitative changes as overexpression of Fbxo45. Furthermore, we showed that the level of the Munc13-1 was regulated by Fbxo45, suggesting that Fbxo45 is critically involved in the regulation of synaptic activity and functions by controlling Munc13-1 protein via ubiquitin dependent proteolysis. It remains to be studied whether there are additional substrates of Fbxo45 involved in the regulation of synaptic activity at the postsynaptic site, because Fbxo45 expresses at not only the presynaptic but also the postsynaptic site.

Fbxo45 is highly conserved among species from *C. elegans* to mammals. The Fbxo45 homologues FSN-1 (*C. elegans*) and DFsn (*Drosophila*) have been shown to be important for synapse formation in the presynaptic neurons by interacting with RING finger-type E3 RPM-1 (*C. elegans*) and Highwire (*Drosophila*), respectively (43, 54). Details on the interaction between Fbxo45 and PAM (protein associated with Myc), RPM-1/Highwire mammalian homologue, will be described elsewhere (45). The *fsn-1* mutant in *C. elegans* and the *DFsn* mutant in *Drosophila* exhibit increased numbers of synapses and abnormal transmission at the neuromuscular junction. *fsn-1*-null animals also exhibit enhanced levels of a receptor-tyrosine kinase, anaplastic lymphoma kinase (ALK), and their phenotype is suppressed by mutations in ALK, suggesting that FSN-1 contributes to the stabilization of synapse formation through a protein degradation pathway (43). In *Drosophila,* DFsn down-regulates the levels of a MAP kinase kinase kinase, Wallenda/dual leucine zipper kinase (DLK), and restrains the growth of synaptic terminals (54). These findings indicate that FSN-1 and DFsn are required for synaptic growth in developing neurons. However, the role of DFsn/FSN-1 in mature neurons is still unclear. Here we showed that Fbxo45 negatively regulated neurotransmission without affecting synapse formation in mature hippocampal neurons. This difference may be because of context-dependent functions of Fbxo45/DFsn/FSN-1 in addition to differences in the species and neuronal regions examined (*i.e.* the hippocampus *versus* the neuromuscular junction). That is, the roles of Fbxo45/DFsn/FSN-1 might switch from those regulating synapse formation to those regulating neurotransmission as the development of the nervous system progresses.

The UPS has recently emerged as an important mechanism for regulating synaptic function. Several ubiquitin ligases are known to regulate presynaptic protein turnover and synaptic efficacy. For example, the E3 ligase SCRAPPER ubiquitinates and mediates the proteasomal degradation of RIM1, a vesicle-priming protein located in the presynaptic active zone. In *Scrapper* knock-out mice, the RIM1 protein levels have an increased half-life, and the mice exhibit enhanced mEPSC frequency. These results indicate that SCRAPPER regulates presynaptic transmitter release by targeting RIM1 for degradation through the UPS (9).

Interestingly, the levels of other presynaptic proteins, including Munc13-1, are also elevated in *Scrapper*-knock-out mice and/or reduced upon SCRAPPER overexpression. However, there is no direct interaction between SCRAPPER and Munc13-1. Therefore, other factors, like the Fbxo45 pathway, appear to regulate the amount of Munc13-1 protein and Munc13-1-dependent neurotransmitter release. A bidirectional pathway between Fbxo45-Munc13-1 and SCRAPPER-RIM1 may cooperatively regulate the priming step of synaptic vesicle release by protein degradation to modulate synaptic transmission. Therefore, an impairment in this pathway may lead to dysfunctional neurotransmission and disruptions in neuronal communication.

Acknowledgments—We thank Dr. M. Matsumoto, Dr. T. Nagai, Dr. M. Watanabe, Dr. M. Uchigashima, Dr. K. O'Donovan, Dr. M. Sakaguchi, Dr. T. Iijima, Dr. M. Yano, Dr. H. Kawahara, Dr. S. Fukami, K. Yasutake, and our colleagues in the Okano, Setou, and Takahashi laboratories for help, encouragement, and advice, K. Tada, R. Tada, and N. Tada for critical advice and continuous support, and Dr. K. Tanaka for valuable reagents.

REFERENCES

1. Li, L., and Chin, L. S. (2003) *Cell. Mol. Life Sci.* **60,** 942–960
2. Sudhof, T. C. (2004) *Annu. Rev. Neurosci.* **27,** 509–547
3. Südhof, T. C. (2008) *Nature* **455,** 903–911
4. Südhof, T. C., and Malenka, R. C. (2008) *Neuron.* **60,** 469–476
5. Inoue, E., Mochida, S., Takagi, H., Higa, S., Deguchi-Tawarada, M., Takao-Rikitsu, E., Inoue, M., Yao, I., Takeuchi, K., Kitajima, I., Setou, M., Ohtsuka, T., and Takai, Y. (2006) *Neuron.* **50,** 261–275
6. DiAntonio, A., and Hicke, L. (2004) *Annu. Rev. Neurosci.* **27,** 223–246
7. Yi, J. J., and Ehlers, M. D. (2005) *Neuron.* **47,** 629–632
8. Yi, J. J., and Ehlers, M. D. (2007) *Pharmacol. Rev.* **59,** 14–39
9. Yao, I., Takagi, H., Ageta, H., Kahyo, T., Sato, S., Hatanaka, K., Fukuda, Y., Chiba, T., Morone, N., Yuasa, S., Inokuchi, K., Ohtsuka, T., Macgregor, G. R., Tanaka, K., and Setou, M. (2007) *Cell* **130,** 943–957
10. Hershko, A., and Ciechanover, A. (1998) *Annu. Rev. Biochem.* **67,** 425–479
11. Voges, D., Zwickl, P., and Baumeister, W. (1999) *Annu. Rev. Biochem.* **68,** 1015–1068
12. Hershko, A., Ciechanover, A., and Varshavsky, A. (2000) *Nat. Med.* **6,** 1073–1081
13. Pickart, C. M. (2001) *Annu. Rev. Biochem.* **70,** 503–533
14. Nakayama, K. I., and Nakayama, K. (2006) *Nat. Rev. Cancer* **6,** 369–381
15. Bai, C., Sen, P., Hofmann, K., Ma, L., Goebl, M., Harper, J. W., and Elledge, S. J. (1996) *Cell* **86,** 263–274
16. Schulman, B. A., Carrano, A. C., Jeffrey, P. D., Bowen, Z., Kinnucan, E. R., Finnin, M. S., Elledge, S. J., Harper, J. W., Pagano, M., and Pavletich, N. P. (2000) *Nature* **408,** 381–386
17. Hatakeyama, S., Kitagawa, M., Nakayama, K., Shirane, M., Matsumoto, M., Hattori, K., Higashi, H., Nakano, H., Okumura, K., Onoé, K., Good, R. A., and Nakayama, K. (1999) *Proc. Natl. Acad. Sci. U.S.A.* **96,** 3859–3863
18. Kitagawa, M., Hatakeyama, S., Shirane, M., Matsumoto, M., Ishida, N., Hattori, K., Nakamichi, I., Kikuchi, A., Nakayama, K., and Nakayama, K. (1999) *EMBO J.* **18,** 2401–2410

19. Nakayama, K. I., and Nakayama, K. (2005) *Semin. Cell Dev. Biol.* **16,** 323–333
20. DiAntonio, A., Haghighi, A. P., Portman, S. L., Lee, J. D., Amaranto, A. M., and Goodman, C. S. (2001) *Nature* **412,** 449–452
21. Schaefer, A. M., Hadwiger, G. D., and Nonet, M. L. (2000) *Neuron.* **26,** 345–356
22. Wan, H. I., DiAntonio, A., Fetter, R. D., Bergstrom, K., Strauss, R., and Goodman, C. S. (2000) *Neuron.* **26,** 313–329
23. Zhen, M., Huang, X., Bamber, B., and Jin, Y. (2000) *Neuron.* **26,** 331–343
24. Kurihara, T., Ozawa, Y., Nagai, N., Shinoda, K., Noda, K., Imamura, Y., Tsubota, K., Okano, H., Oike, Y., and Ishida, S. (2008) *Diabetes* **57,** 2191–2198
25. Wheeler, T. C., Chin, L. S., Li, Y., Roudabush, F. L., and Li, L. (2002) *J. Biol. Chem.* **277,** 10273–10282
26. Chin, L. S., Vavalle, J. P., and Li, L. (2002) *J. Biol. Chem.* **277,** 35071–35079
27. Helton, T. D., Otsuka, T., Lee, M. C., Mu, Y., and Ehlers, M. D. (2008) *Proc. Natl. Acad. Sci. U.S.A.* **105,** 19492–19497
28. Haas, K. F., and Broadie, K. (2008) *Biochim. Biophys. Acta* **1779,** 495–506
29. Darnell, R. B., and Posner, J. B. (2003) *N. Engl. J. Med.* **349,** 1543–1554
30. Musunuru, K., and Darnell, R. B. (2001) *Annu. Rev. Neurosci.* **24,** 239–262
31. Imai, T., Tokunaga, A., Yoshida, T., Hashimoto, M., Mikoshiba, K., Weinmaster, G., Nakafuku, M., and Okano, H. (2001) *Mol. Cell. Biol.* **21,** 3888–3900
32. Sato, S., Chiba, T., Sakata, E., Kato, K., Mizuno, Y., Hattori, N., and Tanaka, K. (2006) *EMBO J.* **25,** 211–221
33. Oshikawa, K., Matsumoto, M., Yada, M., Kamura, T., Hatakeyama, S., and Nakayama, K. I. (2003) *Biochem. Biophys. Res. Commun.* **303,** 1209–1216
34. Akamatsu, W., Okano, H. J., Osumi, N., Inoue, T., Nakamura, S., Sakakibara, S., Miura, M., Matsuo, N., Darnell, R. B., and Okano, H. (1999) *Proc. Natl. Acad. Sci. U.S.A.* **96,** 9885–9890
35. Fukaya, M., Uchigashima, M., Nomura, S., Hasegawa, Y., Kikuchi, H., and Watanabe, M. (2008) *Eur. J. Neurosci.* **28,** 1744–1759
36. Hennou, S., Kato, A., Schneider, E. M., Lundstrom, K., Gähwiler, B. H., Inokuchi, K., Gerber, U., and Ehrengruber, M. U. (2003) *Eur. J. Neurosci.* **18,** 811–819
37. Yano, M., Okano, H. J., and Okano, H. (2005) *J. Biol. Chem.* **280,** 12690–12699
38. Yao, I., Hata, Y., Ide, N., Hirao, K., Deguchi, M., Nishioka, H., Mizoguchi, A., and Takai, Y. (1999) *J. Biol. Chem.* **274,** 11889–11896
39. Yao, I., Hata, Y., Hirao, K., Deguchi, M., Ide, N., Takeuchi, M., and Takai, Y. (1999) *J. Biol. Chem.* **274,** 27463–27466
40. Jin, J., Cardozo, T., Lovering, R. C., Elledge, S. J., Pagano, M., and Harper, J. W. (2004) *Genes Dev.* **18,** 2573–2580
41. Yoshida, K. (2005) *Oncol. Rep.* **14,** 531–535
42. Ponting, C., Schultz, J., and Bork, P. (1997) *Trends Biochem. Sci.* **22,** 193–194
43. Liao, E. H., Hung, W., Abrams, B., and Zhen, M. (2004) *Nature* **430,** 345–350
44. Sakakibara, S., Imai, T., Hamaguchi, K., Okabe, M., Aruga, J., Nakajima, K., Yasutomi, D., Nagata, T., Kurihara, Y., Uesugi, S., Miyata, T., Ogawa, M., Mikoshiba, K., and Okano, H. (1996) *Dev. Biol.* **176,** 230–242
45. Saiga, T., Fukuda, T., Matsumoto, M., Tada, H., Okano, H. J., Okano, H., and Nakayama, K. I. (2009) *Mol. Cell. Biol.* **29,** 3529–3543
46. Rosenmund, C., and Stevens, C. F. (1996) *Neuron.* **16,** 1197–1207
47. Aravamudan, B., Fergestad, T., Davis, W. S., Rodesch, C. K., and Broadie, K. (1999) *Nat. Neurosci.* **2,** 965–971
48. Augustin, I., Rosenmund, C., Südhof, T. C., and Brose, N. (1999) *Nature* **400,** 457–461
49. Richmond, J. E., Weimer, R. M., and Jorgensen, E. M. (2001) *Nature* **412,** 338–341
50. Varoqueaux, F., Sigler, A., Rhee, J. S., Brose, N., Enk, C., Reim, K., and Rosenmund, C. (2002) *Proc. Natl. Acad. Sci. U.S.A.* **99,** 9037–9042
51. Betz, A., Ashery, U., Rickmann, M., Augustin, I., Neher, E., Südhof, T. C., Rettig, J., and Brose, N. (1998) *Neuron.* **21,** 123–136
52. Speese, S. D., Trotta, N., Rodesch, C. K., Aravamudan, B., and Broadie, K. (2003) *Curr. Biol.* **13,** 899–910
53. Deák, F., Liu, X., Khvotchev, M., Li, G., Kavalali, E. T., Sugita, S., and Südhof, T. C. (2009) *J. Neurosci.* **29,** 8639–8648
54. Wu, C., Daniels, R. W., and DiAntonio, A. (2007) *Neural Dev.* **2,** 16
55. Sakakibara, S., Nakamura, Y., Satoh, H., and Okano, H. (2001) *J. Neurosci.* **21,** 8091–8107